# On the Role of Fluoride in Accelerating the Reactions of Dialkylstannylene Acetals

**ARTICLE** *in* THE JOURNAL OF ORGANIC CHEMISTRY · FEBRUARY 2015

Impact Factor: 4.72 · DOI: 10.1021/jo502560q · Source: PubMed



**3 AUTHORS:**

Simiao Lu

Dalhousie University

**1** PUBLICATION **0** CITATIONS

SEE PROFILE

Russell J Boyd

Dalhousie University

**304** PUBLICATIONS **6,030** CITATIONS

SEE PROFILE

Bruce Grindley

Dalhousie University

**138** PUBLICATIONS **1,352** CITATIONS

SEE PROFILE

JOC The Journal of Organic Chemistry

Article

pubs.acs.org/joc

# Role of Fluoride in Accelerating the Reactions of Dialkylstannylene Acetals

Simiao Lu, Russell J. Boyd,* and T. Bruce Grindley*

Department of Chemistry, Dalhousie University, 6274 Coburg Road, P.O. Box 15000, Halifax, Nova Scotia, Canada B3H 4R2

Supporting Information

**ABSTRACT:** The most common method for achieving the regioselective monoalkylation of diols involves formation of dialkylstannylene acetals as intermediates. Reactions of dialkylstannylene acetals with alkyl halides are slow, but rates are enhanced by addition of fluoride or other nucleophiles. The mechanism of the fluoride-accelerated alkylation of dialkylstannylene acetals was studied at several levels of theory in the gas phase, in *N*,*N*-dimethylformamide (DMF) solution, and in DMF solution in the presence of tetramethylammonium ions. The reactive species were adducts involving addition of fluoride to tin. Under the conditions that most closely simulated experiment, reactions from fluoridated monomers and monofluoridated dimers were calculated to have similar activation energies. In the transition states in the rate-determining steps for the two pathways, carbon−oxygen bond formation was between 60 and 75% complete while tin−oxygen bond cleavage was much less advanced, between 6 and 16% complete. A test of Sn−O bond dissociation indicated that the "Sn−O bond cleavage first" mechanism is not a minimum energy pathway.

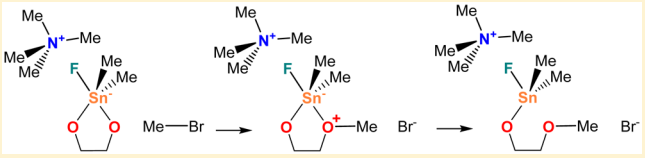


## INTRODUCTION

Dialkylstannylene acetals are intermediates that are commonly employed to achieve regioselective monofunctionalization of diols or polyols, particularly carbohydrates.[1−3] The dialkylstannylene acetal intermediates react with a wide variety of electrophiles, and reactions proceed at higher rates and under milder conditions than with the parent diols. The principal advantage of these reactions, which include acylation, sulfonylation, alkylation, oxidation, and others, is that monosubstitution is obtained, often with high regioselectivity.[1−3] Although these reactions have been known since the 1970s,[4,5] their great utility, as well as debate about their mechanisms and the causes of the regioselectivity, has sparked continuing interest.[6−14] Over the past few years, conditions for some of these reactions have been developed that are catalytic in the organotin reagents.[15−22] Improved understanding of the mechanisms of these reactions could lead to improved regioselectivity and more general catalytic conditions.

Understanding the mechanisms requires clarification of several uncertainties regarding the intermediates in these reactions. A major question is whether monomers or dimers or higher oligomers are the intermediates. Acyclic dialkoxydibutyltin derivatives exist as dimers unless the alkoxyl group is secondary or tertiary.[23,24] The preference for dimerization and further association to oligomers or polymers is greatly increased if the alkoxy groups are joined to form a ring, that is, if the dialkylstannylene acetal is formed from a 1,2- or 1,3-diol (Scheme 1). This increased preference for pentacoordination or hexacoordination of tin is due to the small O−Sn−O bond angle (∼77°) caused by the geometric contraints imposed by having two long Sn−O bonds in the ring.[25] Evidence for this increased oligomerization has come from X-ray crystallographic

**Scheme 1. Formation and Reaction of a Dialkylstannylene Acetal from a 1,2-Diol**

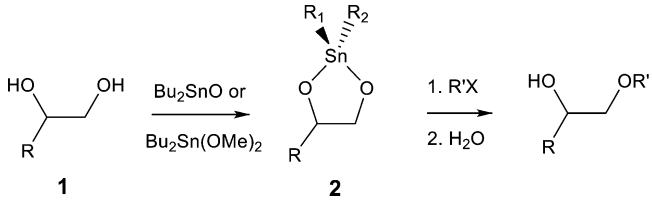


studies, where the derivatives are polymers with hexacoordinate tin if the substituents are small[26−29] or dimers or lower oligomers with pentacoordinate tin or a mixture of pentacoordinate and hexacoordinate tin if they are large.[30−32] In solution, compounds that were polymeric in the solid are mixtures of lower oligomers,[28,33] whereas those that were dimers remain dimeric.[30,34,35]

Alkylation is the most commonly used reaction with these intermediates and is the slowest of the dialkylstannylene reactions. Alkylation reactions are usually performed in the presence of nucleophiles (e.g., halides or amines) that have been found to increase reaction rates sufficiently that they occur under moderate conditions.[36−38] No experimental evidence has been provided as to how these nucleophiles affect the species present in solution, but Whittleton et al. have recently examined this problem theoretically using fluoride as the nucleophile.[39] They examined the three possible equilibria involving addition of fluoride to tin (see Scheme 2). In the gas phase, both the reaction of fluoride with monomers and the

**Received:** November 9, 2014
**Published:** February 10, 2015

  

DOI: 10.1021/jo502560q
J. Org. Chem. 2015, 80, 2989−3002

**Scheme 2. Initial Reactions Involved When Fluoride Is Added to Solutions of Dialkylstannylene Acetals[39]**

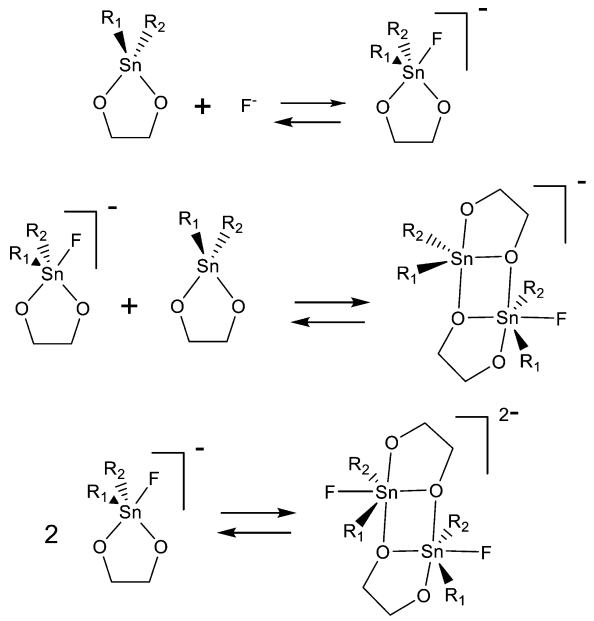

decomposition of difluoridated dimers to give fluoridated monomers were calculated to be highly exothermic. However, if only 0.5 equiv of fluoride was present, monofluoridated dimers were found to be considerably more stable than the mixture of fluoridated monomer and monomer (see Scheme 2).[39] These calculations suggest that both fluoridated dimers and fluoridated monomers could be intermediates in these reactions and that the intermediate could be different depending on the molar ratio of fluoride to dialkylstannylene acetal.

No experimental evidence is available about the pathway by which these fluoridated species (or adducts formed by addition of other nucleophiles) lead to products. Alais and Veyrières suggested, for tributyltin ethers, that the adduct formed by addition of bromide to tin released alkoxide ions that were the reactive nucleophiles,[40] and Nagishima and Ohno[41] indicated that similar mechanisms apply to the adducts formed by addition of fluoride to dibutylstannylene acetals (Scheme 3). Gingras and Harpp[42] suggested that this pathway applies to other compounds containing Sn−O bonds. The idea that Sn−O bond cleavage occurs before electrophile addition has been extended to the reactions of dialkylstannylene acetals conducted in the absence of added nucleophiles recently, using stereoelectronic effects to explain why one of the two Sn−O bonds cleaved regioselectively.[6] This pathway will be called "Sn−O cleavage first" in the following discussion.

An alternative pathway could involve direct reaction of the dialkylstannylene acetal adduct, either as a monomer or as a dimer, with the electrophile. Addition of the nucleophile to tin gives an adduct that bears a negative charge and would be expected to be more nucleophilic than the neutral dialkylstannylene acetal. This pathway will be called the "electrophile addition first" pathway in the following discussion (Scheme 4).

**Scheme 4. "Electrophile Addition First" Reaction Pathway[41]**

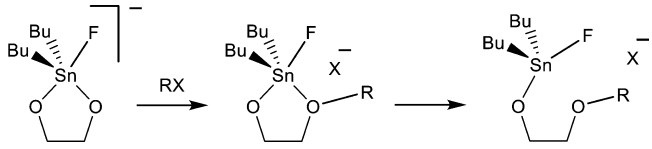

It has been shown that the appropriate choice of computational methods results in the reproduction of the experimental energetics of dialkylstannylene acetal and dialkyldialkoxytin monomer−dimer equilibria.[24,43] Computational methods have also been used to describe their reactions with carbon dioxide.[44−46] Recently, they have been used to evaluate stereoelectronic considerations in the regioselectivity of Sn−O bond cleavage proposed to initiate reactions of stannylene acetals.[6]

To elucidate the mechanism of the reactions both in the gas phase and in solution (*N*,*N*-dimethylformamide, DMF), the pathways for alkylation of ethylene glycol through the adducts of fluoride with dimethylstannylene acetals were evaluated computationally. Dimethylstannylene acetals were chosen to be modeled to allow complete analysis of the reaction pathways. Potential energy surfaces for both monomeric and dimeric tin-containing intermediates were explored with emphasis on comparison of the activation energies, in the gas phase, in a solution with the bulk dielectric constant of DMF, and in this solution in the presence of a tetramethylammonium counterion.

The reactions evaluated are shown in eqs 1−3 in Scheme 5. The alkylation reaction of ethylene glycol with methyl bromide

**Scheme 5. Mono-O-alkylation of Diols through Monomeric and Dimeric Dimethylstannylene Acetals with Added Nucleophiles[a]**

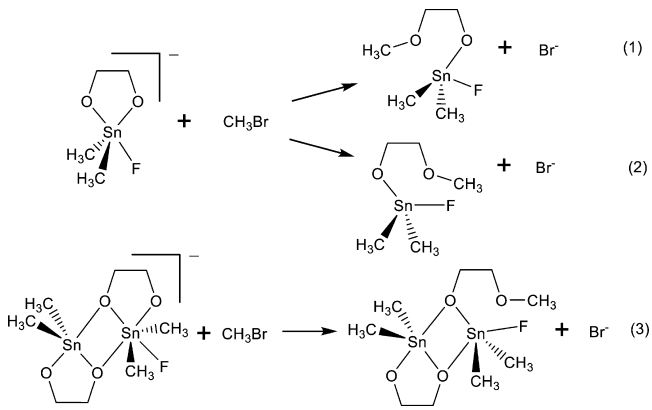

[a]The numbers following each reaction correspond to the reaction pathways discussed in the text.

**Scheme 3. "Sn−O Cleavage First" Reaction Pathway[41]**

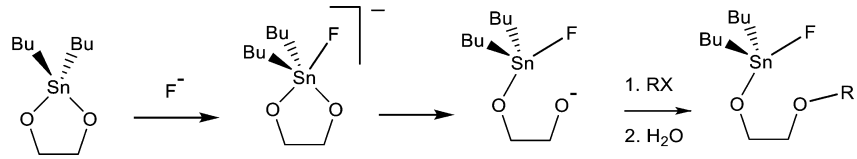



DOI: 10.1021/jo502560q
J. Org. Chem. 2015, 80, 2989−3002

through a monomeric dialkylstannylene acetal was described via two pathways because addition of fluoride to tin results in trigonal bipyramidal geometry at tin in which one oxygen atom is in an equatorial orientation and *syn* to fluoride, while the other is in an apical orientation and *anti* to fluoride. Because both oxygen atoms are activated by the added nucleophile, there are two routes available for reaction with methyl bromide. Formation of the dimer creates two kinds of oxygen atoms: tricoordinate and dicoordinate. The former oxygen atom is connected to two tin atoms from two monomeric units, resulting in steric effects from the four alkyl groups on the two tin atoms that hinder the approach of electrophiles. The dicoordinate oxygen atoms occupy apical positions in the trigonal bipyramidal geometry at tin and are considered to be more reactive.[1] Because the tricoordinate oxygen atom is sterically hindered and is inherently less reactive, only the pathway involving the dicoordinate oxygen atom was evaluated. In Scheme 5, eqs 1 and 2 describe pathways 1 and 2 through the monomeric intermediate, while eq 3 presents the single alkylation pathway via the dimeric adduct.

## COMPUTATIONAL METHODS

Theoretical calculations were carried out with the Gaussian 09 suite of programs.[47] The gas-phase geometry optimizations were conducted using the B3LYP hybrid functional[48−50] combined with the 6-311+G(d,p) basis set for the non-tin atoms. The inclusion of the diffuse functions is important due to the negative charge carried by the nucleophile in the model systems. The Los Alamos National Laboratory double-$\zeta$ basis set (LanL2DZdp) with diffuse and polarization functions[51] and its effective core potential developed by Hay and Wadt[52] were used to treat tin. Transition states were found by Schlegel's synchronous transit-guided quasi-Newton method,[53,54] and the reaction path was followed by using intrinsic reaction coordinate (IRC) calculations.[55,56] In order to obtain reliable thermochemical estimates,[24,43] single-point energy calculations at the MP2[57−60] level (MP2/6-311+G(d,p)//B3LYP-6-311+G(d,p)) were performed on the optimized species. These energies were further corrected by B3LYP Gibbs corrections and ZPVE corrections (zero-point vibrational energy). Calculations were also done with M06-2X[61] because it has been shown to give good results with organotin reactions.[6,45]

Vibrational frequency calculations were carried out to characterize stationary points on the potential energy surfaces (no imaginary frequencies for a local minimum and one for a transition state). All thermochemical parameters were evaluated at default conditions (298.15 K and 1 atm). All of the relative energies displayed from the thermochemical results include ZPVE corrections. Solvent effects were estimated with structures optimized at the B3LYP/6-311+G(d,p)-LanL2DZdp(Sn) level employing the integral equation variant polarizable continuum model in DMF (dielectric constant, 37.219) and water (dielectric constant, 78.3553).

## RESULTS AND DISCUSSION

**Equilibria with Fluoride.** Whittleton et al. recently considered how addition of fluoride to the tin atom of a variety of dibutylstannylene acetals in the gas phase affects the species present (see Scheme 2).[39] To make these results more general, the equilibria of a model dimethylstannylene acetal, 2,2-dimethyl-1,3,2-dioxastannolane, with fluoride were studied in the gas phase, in DMF solution, and in DMF solution containing a tetramethylammonium ion as a counterion. In the adduct resulting from addition of a fluoride ion to the tin atom of the monomer, the tin atom adopts a trigonal bipyramidal geometry with the two methyl groups and one oxygen atom in equatorial orientations and the fluoride and the other oxygen

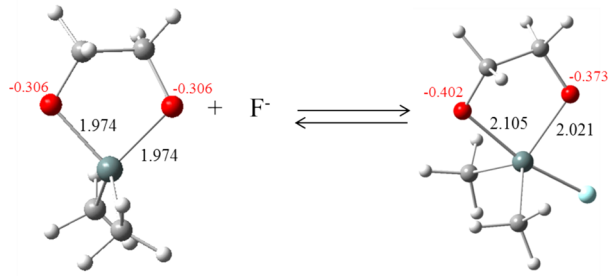


**Figure 1.** Fluoridation of dimethylstannylene acetal monomer. Mulliken charges on oxygen are shown in red, and Sn−O bond lengths are shown in black.

atom apical (see Figure 1). These two oxygen atoms are designated $O_e$ and $O_a$, corresponding to whether the oxygen atom is equatorial or apical in the adduct. Both Sn−O bonds were observed to be slightly elongated on formation of the adduct; Sn−$O_a$ changed from 1.974 to 2.105 Å, and Sn−$O_e$ stretched from 1.974 to 2.021 Å. To evaluate potential changes in reactivity on adduct formation, Mulliken charges on the oxygen atoms were calculated and are displayed in red numbers in Figure 1. Both acetal oxygen atoms became more electron-rich in the adduct, with the apical oxygen atom assuming more negative charge.

The results of the evaluation of the first two equilibria shown in Scheme 2 under various conditions are given in Table 1. Two theoretical techniques were applied for the evaluation. In the first method, MP2 single-point energy calculations were conducted based on structures optimized with B3LYP. These MP2 energies were further corrected by B3LYP ZPVE corrections, Gibbs corrections, enthalpy corrections, and MP2 basis set superposition error (BSSE) corrections, where M, $MF^-$, and $DF^-$ represent the monofluoridated monomer, fluoridated monomer, and monofluoridated dimer, respectively (Scheme 2). These equilibria reactions are also evaluated using M06-2X with BSSE corrections. The corresponding equations are shown below:

1. Relative energy of monofluoridation

$$\Delta E = E_{MF}^- - E_F^- - E_M$$

$$\Delta H = H_{MF}^- - H_F^- - H_M$$

$$\Delta G = G_{MF}^- - G_F^- - G_M$$

2. Relative energy of monofluoridated dimerization

$$\Delta E = E_{DF}^- - E_{MF}^- - E_M$$

$$\Delta H = H_{DF}^- - H_{MF}^- - H_M$$

$$\Delta G = G_{DF}^- - G_{MF}^- - G_M$$

The results in the gas phase for these equilibria are similar to those previously observed by Whittleton at al. for dibutylstannylene acetals.[39] Whittleton at al. also evaluated the equilibria between two monofluoridated monomers and the difluoridated dimer and found that the difluoridated dimer was very much less stable. We attempted to evaluate the analogous equilibrium here but were unable to find a structure for the difluoridated dimer that was a minimum. We have assumed that the difluoridated dimer is not an intermediate in the alkylation reaction. This position is based on the assumption that each half of a difluoridated dimer would have a reactivity similar to


DOI: 10.1021/jo502560q
J. Org. Chem. 2015, 80, 2989−3002

**Table 1. Summary of Relative Energetics of Equilibria Involved When Fluoride Is in the Presence of 2,2-Dimethyl-1,3,2-dioxastannolane[a]**

| conditions | reaction | $\Delta E$ (kJ mol$^{-1}$) | $\Delta H$ (kJ mol$^{-1}$) | $\Delta S$ (J/mol) | $\Delta G$ (kJ mol$^{-1}$)[b] |
|---|---|---|---|---|---|
| in gas phase using MP2//B3LYP | monomer fluoridation | −271.3 | −273.1 | −110.0 | −240.3 |
| | monofluoridated dimerization | −126.7 | −126.1 | −193.2 | −68.5 |
| in gas phase using M06-2X | monomer fluoridation | −289.8 | −293.8 | −132.5 | −254.3 |
| | monofluoridated dimerization | −161.3 | −159.0 | −178.0 | −106.0 |
| in DMF using MP2//B3LYP | monomer fluoridation | −112.1 | −114.1 | −114.9 | −79.8 |
| | monofluoridated dimerization | −73.2 | −78.1 | −207.6 | −16.2 |
| in DMF using M06-2X | monomer fluoridation | −129.3 | −127.3 | −79.3 | −103.6 |
| | monofluoridated dimerization | −99.3 | −95.1 | −159.8 | −47.5 |
| in DMF with cation using MP2//B3LYP | monomer fluoridation | −113.9 | −111.9 | −146.9 | −68.2 |
| | monofluoridated dimerization | −2.5 | −2.7 | −204.6 | 58.3 |
| in DMF with cation using M06-2X | monomer fluoridation | −128.0 | −122.8 | −132.2 | −83.4 |
| | monofluoridated dimerization | −47.6 | −44.7 | −165.8 | 4.7 |

[a]Equilibria 1−3 are as shown in Scheme 2. [b]At 298 K.

**Table 2. Selected Geometric Parameters for the Reactant Complexes (RC), Transition States (TS), and Product Complexes (PC) from Pathways 1 and 2 Using B3LYP/6-311+G(d,p)-LanL2DZdp(Sn)[a]**

| | pathway 1 | | | pathway 2 | | |
|---|---|---|---|---|---|---|
| structural feature | RC1 | TS1 | PC1 | RC2 | TS2 | PC2 |
| $r$(Sn,O$_a$) (Å) | 2.123 | 2.215 | 2.643 | 2.092 | 2.069 | 1.983 |
| $r$(Sn,O$_e$) (Å) | 2.014 | 1.998 | 1.995 | 2.027 | 2.095 | 2.583 |
| $r$(Sn,F) (Å) | 2.004 | 1.984 | 1.952 | 2.024 | 1.994 | 1.933 |
| $r$(O,H) (Å) | 2.040 | | | | | |
| $r$(F,H) (Å) | | | | 2.100 | 2.260 | |
| $r$(O,C$_M$) (Å) | 3.107 | 2.028 | 1.431 | 2.977 | 1.948 | 1.438 |
| $r$(C$_M$,Br) (Å) | 1.985 | 2.437 | 3.735 | 2.001 | 2.537 | 3.864 |
| $r$(H,Br) (Å) | | | 2.655 | | | 2.728 |
| $r$(H′,Br) (Å) | | | | | | 2.827 |
| ∠(O$_a$,Sn,O$_e$) (deg) | 80.3 | 78.3 | 70.4 | 80.7 | 78.2 | 71.5 |
| ∠(O$_e$,Sn,F) (deg) | 88.2 | 90.0 | 94.4 | 85.3 | 82.0 | 76.7 |
| ∠(C,Sn,C′) (deg) | 119.2 | 121.8 | 127.8 | 119.5 | 121.4 | 113.5 |
| ∠(O,C$_M$,Br) (deg) | 119.3 | 178.6 | 101.6 | 174.6 | 176.3 | 89.9 |
| ∠(C$_M$,C,O,Sn) (deg) | 164.9 | −151.9 | −146.7 | −1.2 | −161.6 | −149.8 |
| ∠(Br,C,O,Sn) (deg) | 177.2 | −152.7 | −97.3 | −3.5 | −162.5 | −158.8 |

[a]The $r$(Sn,O$_a$) and $r$(Sn,O$_e$) refer to the intramolecular bonds between tin and apical and equatorial atoms, respectively (see Figures 1 and 2). The $r$(H,Br) and $r$(H′,Br) in the PC2 column refer to the hydrogen bonds between the bromide atom and the hydrogen atoms from the methylene group and methyl group, separately. C$_M$ indicates the carbon atom from the methyl group of methyl bromide.

that of the fluorine-containing half of a monofluoridated dimer, but the difluoridated dimer would be very much less populated. An alternative intermediate could be the difluoridated monomer ($MF_2^{-2}$). This intermediate would be expected to be much less stable than the monofluoridated monomer but probably much more reactive. If its reaction or its formation were rate-determining, the kinetics would show a dependence on the concentration of $F^-$ to the second power. Qualitative kinetics suggest that the dependence of rate on concentration of fluoride is closer to first order,[7] ruling out this intermediate.

In DMF solution, the Gibbs energy for the addition of fluoride to the monomer decreases to about one-third of the gas-phase value but is still substantial. A significant decrease in the relative stability of the fluoridated monomer is expected because a polar solvent will stabilize the localized charge on the fluoride ion more than it does the delocalized charge on the fluoridated monomer. In the presence of a cation in DMF, the position of equilibrium 2 was calculated to reverse to favor the monomer and the fluoridated monomer over the monofluoridated dimer. The calculated positions of the equilibria are not sufficiently in favor of the starting materials to rule out the monofluoridated dimer as an intermediate in alkylation reactions. The tetrabutylammonium ion remained close to the most electronegative atom, F, in the optimized structures.

**Monomeric Reaction Pathways.** Optimized structures were calculated with B3LYP/6-311+G(d,p) along two pathways leading from the two different oxygen atoms in the monomeric adducts in the gas phase. Pathway 1 corresponds to the apical oxygen atom acting as the nucleophile, while pathway 2 uses the equatorial oxygen atom as the nucleophile. Geometric parameters are displayed in Table 2. As the methyl bromide approaches the dimethylstannylene acetal adduct, a potential energy minimum, the reactant complex, is formed in both pathways. In the approach of the methyl bromide along pathway 1 (Figure 3), a hydrogen bond (2.040 Å) is formed between the apical oxygen atom and one of the hydrogen atoms from the methyl group.

A second reaction complex that did not have a hydrogen bond is also found; this RC1 structure was confirmed by a scan job that started from the optimized transition state (TS1) and gradually separated the acetal and the electrophile. In TS1, the optimized geometry at the methyl carbon is that of the well-known transition state structure of the $S_N2$ reaction with a partially pentacoordinate carbon having trigonal bipyramidal geometry.[62,63] The Sn−O$_a$ bond lengthens by about 4% on moving from RC1 (2.123 Å) to TS1 (2.215 Å). An IRC calculation was used to follow the pathway from this transition structure (TS1) to the product complex. In the product complex, the Sn−O$_a$ bond is considerably longer (2.643 Å), but the Sn−F bond is slightly shorter (1.952 Å). Two hydrogen bonds stabilized the product complex (PC1) in the gas phase.

The reactant complex (RC2) formed along pathway 2 is stabilized by a hydrogen bond between the fluoride and one hydrogen atom of the methyl group (2.100 Å). In the transition state (TS2), the partially pentacoordinate carbon of the methyl group adopts the trigonal bipyramidal structure of the $S_N2$ transition state. As with pathway 1, the distance between the Sn atom and the reacting O atom, O$_e$ in this case, increases on


DOI: 10.1021/jo502560q
J. Org. Chem. 2015, 80, 2989−3002

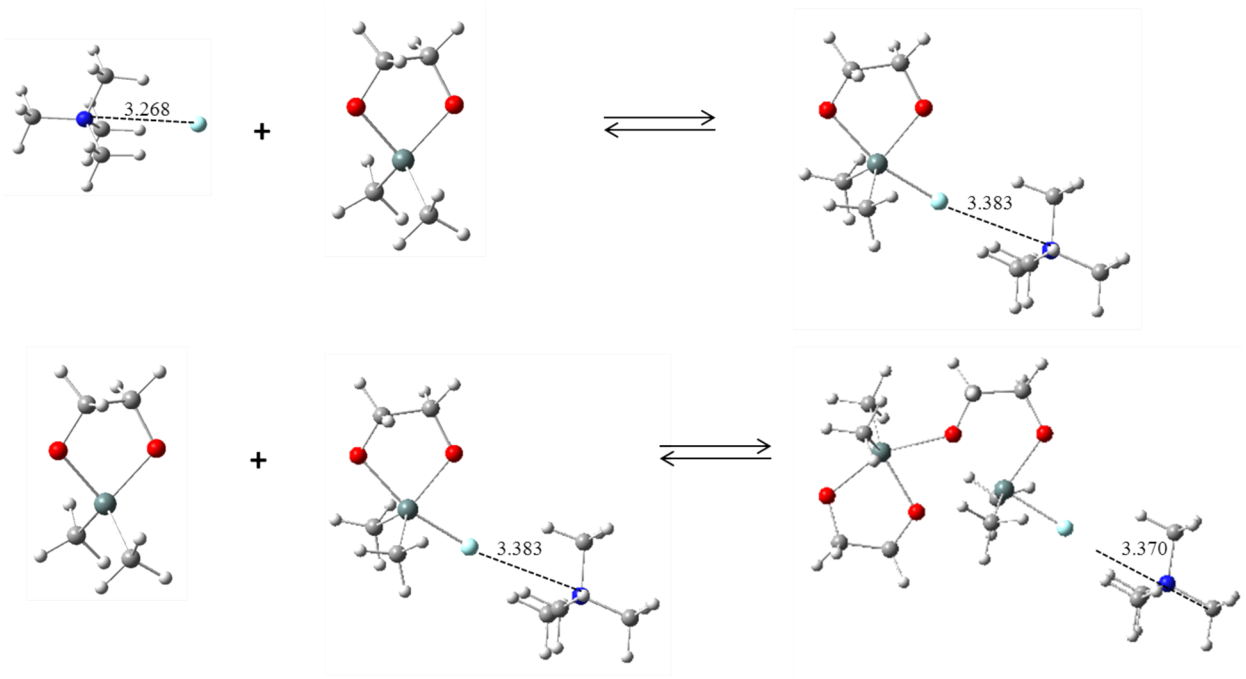


**Figure 2.** Optimized structures in DMF in the presence of the tetramethylammonium ion.

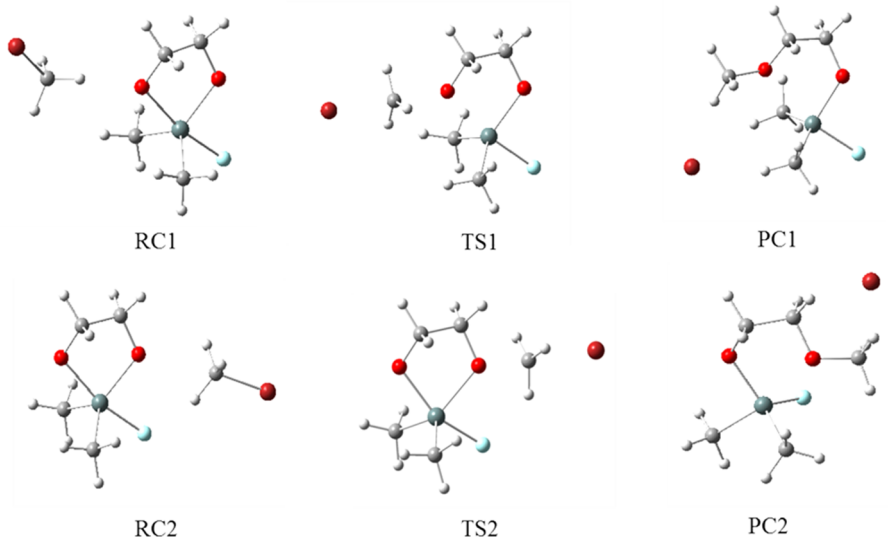


**Figure 3.** Structures of reactant complexes (RC), transition states (TS), and product complexes (PC) along reaction pathways 1 and 2 via monomeric intermediates with an added fluoride in the gas phase.

**Table 3. Comparison of Critical Bond Lengths (Å) in Reactant Complexes (RC), Transition States (TS), and Product Complexes (PC)**

| pathway | bond | RC (Å) | TS (Å) | PC (Å) | PC−RC (Å) | TS−RC (Å) | % change |
|---|---|---|---|---|---|---|---|
| 1 | C−Br | 1.985 | 2.437 | 3.735 | 1.750 | 0.452 | 23 |
| | $Sn-O_a$ | 2.123 | 2.215 | 2.643 | 0.520 | 0.092 | 18 |
| | $O_a-C_M$ | 3.107 | 2.028 | 1.431 | −1.676 | −1.079 | 64 |
| 2 | C−Br | 2.001 | 2.537 | 3.864 | 1.863 | 0.536 | 29 |
| | $Sn-O_e$ | 2.027 | 2.095 | 2.583 | 0.556 | 0.068 | 12 |
| | $O_e-C_M$ | 2.977 | 1.948 | 1.438 | −1.539 | −1.029 | 67 |
| 3 | C−Br | 1.992 | 2.574 | 3.901 | 1.808 | 0.536 | 32 |
| | $Sn-O_e$ | 2.008 | 2.106 | 2.247 | 0.239 | 0.098 | 33 |
| | $O_e-C_M$ | 3.116 | 1.912 | 1.449 | −1.667 | −1.204 | 72 |



DOI: 10.1021/jo502560q
*J. Org. Chem.* 2015, 80, 2989−3002

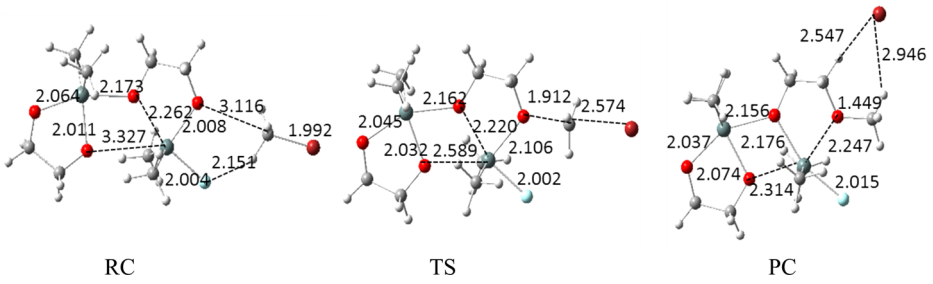


**Figure 4.** Geometries of structures along the dimer reaction pathway in the gas phase obtained using B3LYP/6-311+G(d,p)-LanL2DZdp(Sn). Selected interatomic distances (Å) are shown.

**Table 4. Selected Geometric Parameters for the Reactant Complexes (RCm), Transition States (TSm), and Product Complexes (PCm) from Pathways 1 and 2 Using M06-2X/6-311+G(d,p)-LanL2DZdp(Sn)[a]**

| | pathway 1 | | | | pathway 2 | |
|---|---|---|---|---|---|---|
| structural feature | RCm1 | TSm1 | PCm1 | RCm2 | TSm2 | PCm2 |
| $r(Sn,O_a)$ (Å) | 2.103 | 2.175 | 2.625 | 2.077 | 2.057 | 1.973 |
| $r(Sn,O_e)$ (Å) | 1.998 | 1.987 | 2.050 | 2.012 | 2.071 | 2.499 |
| $r(Sn,F)$ (Å) | 1.986 | 1.970 | 1.946 | 2.006 | 1.980 | 1.922 |
| $r(O,H)$ (Å) | 2.099 | | | | | |
| $r(F,H)$ (Å) | | | | 2.093 | 2.222 | |
| $r(O,C_M)$ (Å) | 3.082 | 1.953 | 1.411 | 2.751 | 1.924 | 1.430 |
| $r(C_M,Br)$ (Å) | 1.961 | 2.394 | 3.753 | 1.978 | 2.447 | 3.778 |
| $r(H,Br)$ (Å) | | | 2.881 | | | 2.697 |
| $r(H',Br)$ (Å) | | | | | | 2.756 |
| $\angle(O_a,Sn,O_e)$ (deg) | 80.8 | 78.8 | 70.8 | 80.9 | 78.7 | 72.7 |
| $\angle(O_e,Sn,F)$ (deg) | 88.8 | 90.2 | 98.6 | 85.3 | 81.7 | 75.1 |
| $\angle(C,Sn,C')$ (deg) | 120.1 | 121.2 | 159.7 | 120.7 | 122.7 | 113.9 |
| $\angle(O,C_M,Br)$ (deg) | 129.5 | 180.0 | 78.4 | 177.5 | 176.7 | 112.5 |
| $\angle(C_M,C,O,Sn)$ (deg) | −120.5 | 175.7 | −140.4 | −164.7 | −157.8 | −130.5 |
| $\angle(Br,C,O,Sn)$ (deg) | −149.0 | 175.7 | −17.5 | −165.5 | −158.4 | −151.0 |

[a]The $r(Sn,O_a)$ and $r(Sn,O_e)$ refer to the intramolecular bonds between tin and apical and equatorial atoms, respectively (see Figures 1 and 2). The $r(H,Br)$ and $r(H',Br)$ in the PCm2 column refer to the hydrogen bonds between the bromide atom and the hydrogen atoms from the methylene group and methyl group, separately. $C_M$ indicates the carbon atom from the methyl group of methyl bromide.

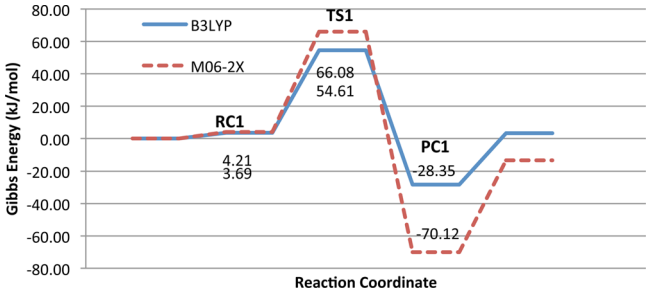


**Figure 5.** Potential energy profile for pathway 1 of the alkylation reaction in the gas phase calculated using (1) the B3LYP/6-311+G(d,p)-LanL2DZdp(Sn) basis set and (2) the M06-2X/6-311+G(d,p)-LanL2DZdp(Sn) basis set. RC1, TS1, and PC1 are abbreviations for the reactant complex, transition state, and product complex.

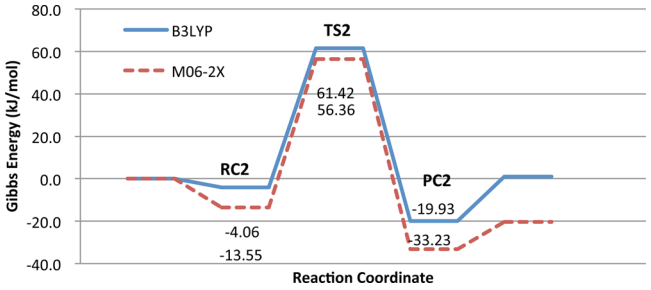


**Figure 6.** Potential energy profile for pathway 2 of the alkylation reaction in the gas phase calculated using (1) the B3LYP/6-311+G(d,p)-LanL2DZdp(Sn) basis set and (2) the M06-2X/6-311+G(d,p)-LanL2DZdp(Sn) basis set. See Figure 5 for abbreviations.

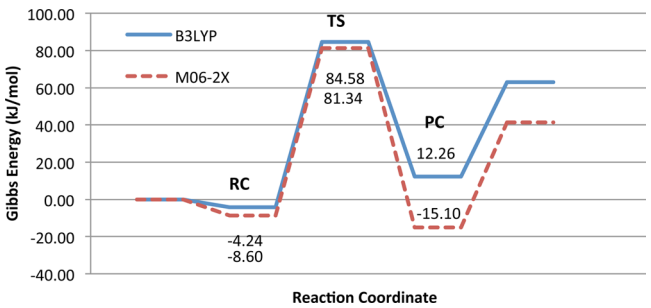


**Figure 7.** Potential energy profile for the pathway of the alkylation reaction via the dimeric intermediate with an added fluoride in the gas phase calculated using (1) the B3LYP/6-311+G(d,p)-LanL2DZdp-(Sn) basis set and (2) the M06-2X/6-311+G(d,p)-LanL2DZdp(Sn) basis set. See Figure 5 for abbreviations.

**Table 5. Summary of Activation Energies $\Delta G^{\ddagger}$ and Reaction Energies $\Delta G_{rxn}$ (kJ mol$^{-1}$) for Each Reaction Pathway in the Gas Phase**

| method | pathway | $\Delta G^{\ddagger a}$ | $\Delta G_{rxn}{}^{b}$ | $\Delta G^{\ddagger c}$ |
|---|---|---|---|---|
| B3LYP | from monomer 1 | 50.9 | 3.3 | 54.6 |
| | from monomer 2 | 65.5 | 1.0 | 61.4 |
| | from dimer | 88.8 | 63.0 | 84.6 |
| M06-2X | from monomer 1 | 61.9 | −13.3 | 66.1 |
| | from monomer 2 | 69.9 | −20.4 | 56.4 |
| | from dimer | 90.0 | 41.4 | 81.3 |

[a]Gibbs energy difference between transition states and the corresponding reactant complexes. [b]Gibbs energy difference between products and reactants. [c]Gibbs energy difference between transition states and the corresponding reactants.

moving from the reactant complex to the transition state by 0.068 Å (~3%). The product complex (PC2) is stabilized by two hydrogen bonds as was PC1. Hydrogen bonds are formed



DOI: 10.1021/jo502560q
J. Org. Chem. 2015, 80, 2989−3002

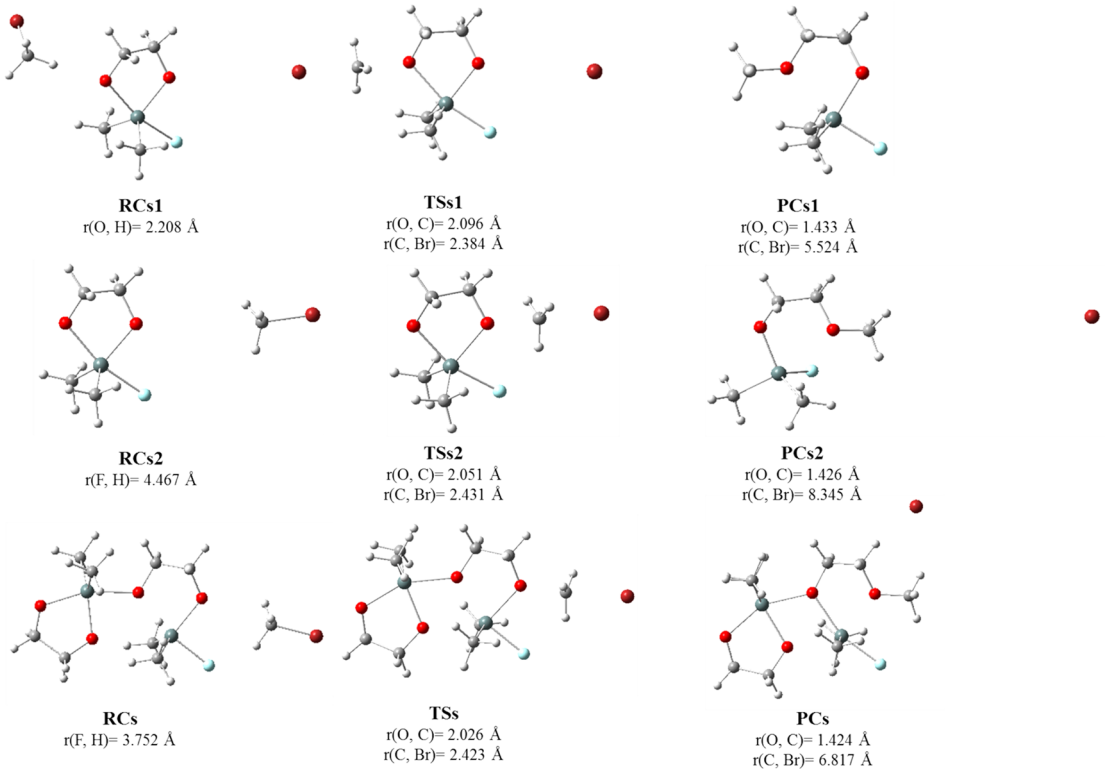


**Figure 8.** Optimized structures of systems involved in monomer pathways 1 and 2 and in the dimer pathway in a medium with the dielectric constant of DMF as calculated by B3LYP.

**Table 6. Selected Interatomic Distances (Å) for Structures Calculated by M06-2X in DMF**

| | pathway 1 | | | pathway 2 | | | pathway 3 | | |
|---|---|---|---|---|---|---|---|---|---|
| structure | RCmd1 | TSmd1 | PCmd1 | RCmd2 | TSmd2 | PCmd2 | RCmd | TSmd | PCmd |
| $r$(O,H) | 2.186 | | | | | | | | |
| $r$(F,H) | | | | 3.441 | 2.210 | | 3.449 | 2.139 | |
| $r$(O,$C_M$) | 3.222 | 2.039 | 1.427 | 2.857 | 1.997 | 1.422 | 2.833 | 2.013 | 1.417 |
| $r$($C_M$,Br) | 1.954 | 2.332 | 3.616 | 1.962 | 2.380 | 3.793 | 1.962 | 2.369 | 4.410 |
| $r$(H,Br) | | | | | | | | | 3.334 |
| $r$(H′,Br) | | | | | | | | | 3.827 |

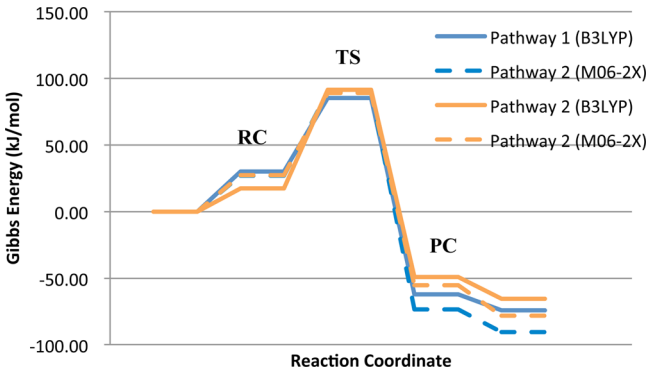


**Figure 9.** Potential energy profile for the pathway of alkylation reaction via monomeric intermediates bearing an added fluoride ion in DMF calculated using the B3LYP/6-311+G(d,p)-LanL2DZdp(Sn) basis set and M06-2X/6-311+G(d,p)-LanL2DZdp(Sn). For abbreviations, see Figure 5.

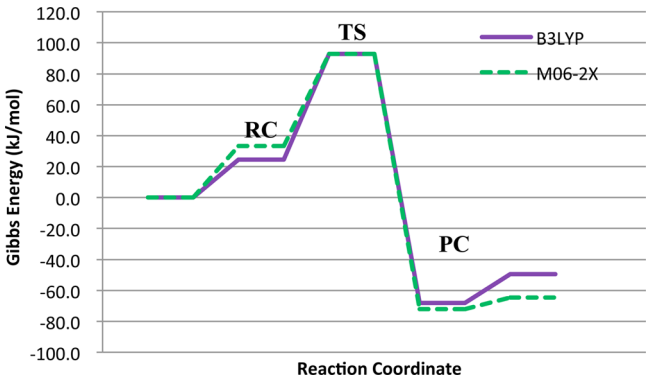


**Figure 10.** Potential energy profile for the pathway of the alkylation reaction via a dimeric intermediate with an added fluoride in DMF calculated using the B3LYP/6-311+G(d,p)-LanL2DZdp(Sn) basis set and M06-2X/6-311+G(d,p)-LanL2DZdp(Sn). For abbreviations, see Figure 5.

between the bromide ion and hydrogen atoms of the methyl group and a methylene group ($r$(H,Br) = 2.728 Å and $r$(H′,Br) = 2.827 Å). The ring structure is distorted with significant elongation of the Sn−$O_e$ bond (2.583 Å).



DOI: 10.1021/jo502560q
J. Org. Chem. 2015, 80, 2989−3002

**Table 7. Summary of Activation Energies from Reactant Complexes ($\Delta G^{\ddagger}_1$), Reaction Energies ($\Delta G_{rxn}$), and Overall Activation Energies ($\Delta G^{\ddagger}_0$) for Each Reaction Pathway Calculated in DMF and in Water**

| pathway | solvent (method) | $\Delta G^{\ddagger}_1$ [a] (kJ mol$^{-1}$) | $\Delta G_{rxn}$ [b] (kJ mol$^{-1}$) | $\Delta G^{\ddagger}_0$ [c] (kJ mol$^{-1}$) |
|---|---|---|---|---|
| monomer pathway 1 | DMF (B3LYP) | 55.2 | −74.4 | 85.4 |
| | water (B3LYP) | 55.9 | −74.9 | 86.9 |
| | DMF (M06-2X) | 62.8 | −90.5 | 89.7 |
| monomer pathway 2 | DMF (B3LYP) | 74.0 | −65.6 | 91.5 |
| | water (B3LYP) | 70.5 | −65.7 | 92.1 |
| | DMF (M06-2X) | 61.7 | −78.2 | 89.0 |
| dimer pathway | DMF (B3LYP) | 68.3 | −49.6 | 92.8 |
| | water (B3LYP) | 68.9 | −51.4 | 92.9 |
| | DMF (M06-2X) | 59.6 | −64.5 | 93.0 |

[a]Gibbs energy difference between transition states and corresponding reactant complexes. [b]Gibbs energy difference between products and reactants. [c]Gibbs energy difference between transition states and corresponding reactants.

**Table 8. Comparison of Mulliken Charges Calculated with B3LYP for the Fluoridated Monomer with and without a Tetramethylammonium Ion Present**

| | Mulliken charges (au) | |
|---|---|---|
| atom | without a cation | with a cation |
| F | −0.57 | −0.42 |
| $O_e$ | −0.50 | −0.48 |
| $O_a$ | −0.47 | −0.46 |

Through both pathways, the Sn−F bonds shrink when proceeding from the RC to the TS to the PC (see Table 2). The O−Sn−O bond angle closes in both cases in this alkylation process (pathway 1: 80.3 to 70.4°; pathway 2: 80.7 to 71.5°). However, the O−Sn−X angle opens from 88.2 to 94.4° in pathway 1, while it closes from 85.3 to 76.7° in pathway 2.

An estimate of the relative importance of C−O bond formation versus Sn−O bond cleavage in the transition state can be obtained by comparing the bond lengths in the reactant and product complexes with those in the transition state (Table 3). In the transition state along pathway 1, the bond between the $O_a$ and the methyl carbon is about 64% formed, while the $O_a$ to the tin bond is about 18% broken, suggesting that, while both events are occurring, the pathway is closer to the "electrophile addition first" pathway. Pathway 2 is similar but is slightly closer to the "electrophile addition first" pathway, in that the C−O bond is 67% formed and the Sn−O bond is 12% broken (see Table 3).

**Dimeric Reaction Pathway (Pathway 3).** As explained in the Introduction, only one pathway was examined for the dimeric intermediate (Figure 4). The geometry of the approach with respect to the added nucleophile is similar to that in pathway 2 for monomeric intermediates.

In the presence of an added fluoride, the symmetry of the dimer structure is lost. In the reactant complex, the intramonomer Sn−$O_e$ bond from the fluoridated monomer lengthens slightly, but the Sn−O intermonomer bond involving the coordinated tin atom from the fluoridated monomer lengthens more, by about 50% of the original separation. The intramonomer Sn−$O_a$ bond from the fluoridated monomer and the other intermonomer Sn−O bond shrink slightly. A hydrogen bond (2.151 Å) is formed between the fluoride and a methyl hydrogen atom in the reactant complex. In the conversion to the transition state, the intramonomer Sn−O bond to the coordinated tin atom lengthens ($r$(Sn−$O_a$) from 2.008 to 2.106 Å), but the intermonomer Sn−O bond to the coordinated tin atom shortens significantly (3.327 to 2.589 Å). In the transition state, the methyl group keeps its arrangement from the reactant complex, and the carbon center becomes pentacoordinate with the regular trigonal bipyramidal geometry of the $S_N2$ transition state. Based on the C−O bond length changes, this pathway is very close to an "electrophile first" pathway, with the C−O bond being 72% formed in the TS. Because this is a dimer, the Sn−O bond length changes are more complex. As with monomer pathway 2, two hydrogen bonds (2.547 and 2.946 Å) were observed in the gas phase. For more geometric parameters, see Supporting Information.

**Comparison of Geometries Obtained with the M06-2X Functional.** When the structures optimized with B3LYP and M06-2X functionals were compared, small differences of the geometric parameters were observed. For example, Table 4 displays the geometric parameters of both monomer pathways using M06-2X/6-311+G(d,p)-LanL2DZdp(Sn). Except for the hydrogen bond lengths in RCm1 and PCm1 and one Sn−O bond from PCm1, all other bonds are slightly shorter in the M06-2X-optimized structures. The largest differences are the hydrogen bond predictions and the placement of the methyl bromide in the reactant complexes. Although it is well-known that B3LYP underestimates London dispersion,[64] this method still predicts reasonable numbers for hydrogen bond lengths. M06-2X gives slightly longer distances between the nucleophilic oxygen atoms and the methyl hydrogen atoms (B3LYP, 2.040 Å; M06-2X, 2.099 Å) and between bromide and hydrogen atoms from the methyl group (B3LYP, 2.655 Å; M06-2X, 2.881 Å). On the other hand, when the last two dihedral angles of RC1 (Table 3) and RCm1 (Table 4) are compared, the hydrogen bond lengths are different and the methyl bromide is oriented differently in these reactant complexes. Furthermore, B3LYP predicted a PC2 structure with the leaving group bromide forming hydrogen bonds with hydrogen atoms from the top methylene and methyl group. In comparison, in the PCm2 structure, the bromide ion moved during minimization over a presumably flat energy surface to a position to the bottom right of the structure pictured in Figure 3, where it formed hydrogen bonds to the O−Me methyl group and to a Sn−Me methyl group. Comparisons of percentage changes in bond lengths between product complexes and reagent complexes versus changes in transition states and reagent complexes are very similar to those obtained with B3LYP calculations that are outlined in Table 3.

**Thermochemistry.** Thermochemical results obtained from B3LYP and M06-2X will be compared. MP2 single-point energy calculations based on the B3LYP-optimized species were also applied. However, a very large energy difference between reactants and reactant complexes was found, which suggests that B3LYP MP2-corrected Gibbs energies are unreliable for predicting organotin-mediated alkylation of diols, similar to the conclusions drawn for reactions of dialkylstannylene acetals with carbon dioxide.[45] In addition,


DOI: 10.1021/jo502560q
J. Org. Chem. 2015, 80, 2989−3002

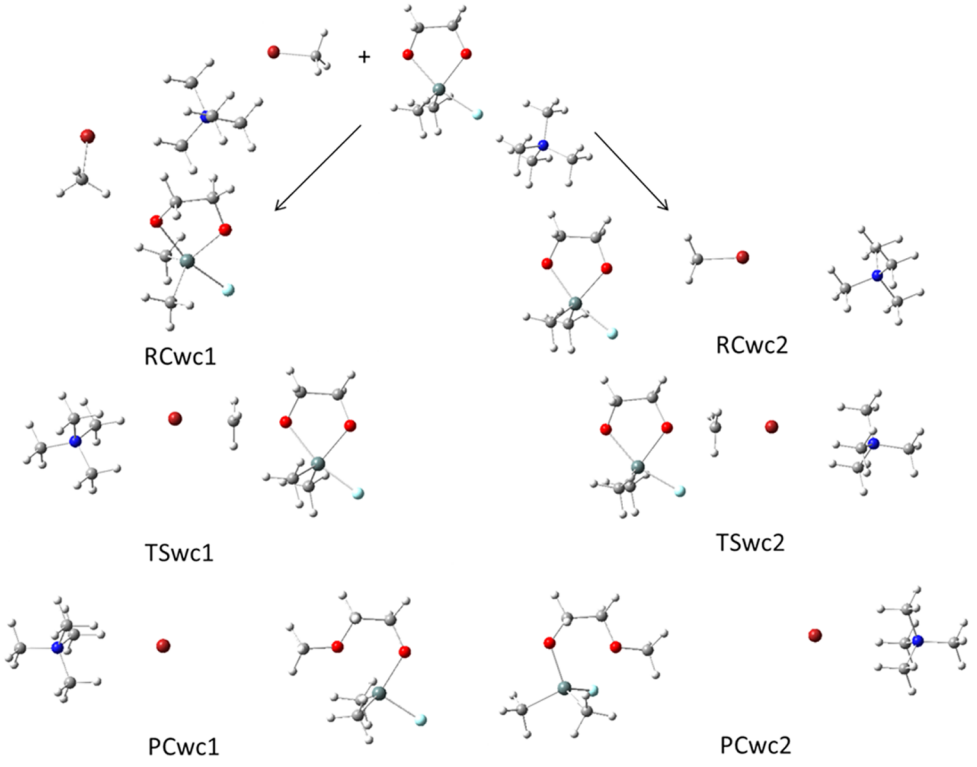


**Figure 11.** Optimized geometries of the alkylation reaction of the monofluoridated dimethylstannylene acetal monomer in the presence of the tetramethylammonium ion in DMF were calculated using the B3LYP/6-311+G(d,p)-LanL2DZdp(Sn) basis set. Two pathways (pathway 1, reactant complex (RCwc1), transition state (TSwc1), and product complex (PCwc1); pathway 2, reactant complex (RCwc2), transition state (TSwc2), and product complex (PCwc2)) are indicated in the figure.

**Table 9. Selected Geometric Data of Optimized Structures in Monomeric Pathways in DMF Containing Tetramethylammonium Ions Using the B3LYP/6-311+G(d,p)-LanL2DZdp(Sn) Basis Set**

| | pathway 1 | | | pathway 2 | | |
|---|---|---|---|---|---|---|
| structure | RCwc1 | TSwc1 | PCwc1 | RCwc2 | TSwc2 | PCwc2 |
| $r$(Sn,O$_a$) (Å) | 2.098 | 2.164 | 2.500 | 2.098 | 2.077 | 1.968 |
| $r$(Sn,O$_e$) (Å) | 2.025 | 2.010 | 1.979 | 2.025 | 2.072 | 2.761 |
| $r$(Sn,F) (Å) | 2.055 | 2.034 | 1.976 | 2.056 | 2.047 | 1.950 |
| $r$(O,H) (Å) | 2.214 | | | | | |
| $r$(F,H) (Å) | | | | 4.149 | 2.153 | |
| $r$(O,C$_M$) (Å) | 3.302 | 2.114 | 1.432 | 3.992 | 2.071 | 1.426 |
| $r$(C$_M$,Br) (Å) | 1.982 | 2.368 | 5.613 | 1.976 | 2.411 | 6.983 |
| $r$(Br, N) (Å) | 6.120 | 4.402 | 4.254 | 6.094 | 4.362 | 4.250 |
| ∠(O$_a$,Sn,O$_e$) (deg) | 80.7 | 79.2 | 73.1 | 80.7 | 79.1 | 68.9 |
| ∠(O$_e$,Sn,F) (deg) | 84.1 | 85.5 | 91.3 | 83.9 | 81.7 | 74.4 |
| ∠(C,Sn,C′) (deg) | 121.0 | 122.9 | 125.7 | 120.8 | 123.2 | 117.8 |
| ∠(O,C$_M$,Br) (deg) | 107.6 | 179.1 | 158.6 | 177.5 | 179.2 | 161.9 |
| ∠(C$_M$,Br,N) (deg) | 123.1 | 150.3 | 176.7 | 168.0 | 166.5 | 170.2 |
| ∠(C$_M$,C,O,Sn) (deg) | 110.1 | −146.1 | −148.3 | −168.4 | −150.3 | −138.8 |
| ∠(Br,C,O,Sn) (deg) | 152.6 | −146.6 | −166.6 | −168.0 | −150.7 | −154.1 |
| ∠(O,C$_M$,Br,N) (deg) | 17.1 | 60.2 | 49.5 | −47.1 | 21.7 | 87.9 |

these unreasonable energies were also discovered when the effects of solvents were included. The schematic potential energy surfaces of the alkylation reactions via the monomeric intermediates in both pathways and via the dimeric intermediates in the gas phase are shown in Figures 5−7.

The energy profile for a $S_N2$ reaction calculated in the gas phase usually exhibits a characteristic double-well potential curve, which includes three stages: the reaction complex or the ion−molecule complex, the transition state, and the product complex.[62,63] The thermochemical results calculated by B3LYP and M06-2X for these systems provide similar double-well potential curves. However, the reactant complexes form in the first step with a slight increase in energy (B3LYP, 3.7 kJ mol$^{-1}$; M06-2X, 4.2 kJ mol$^{-1}$). These complexes overcome reaction barriers (B3LYP, 54.6 kJ mol$^{-1}$; M06-2X, 66.1 kJ mol$^{-1}$), and the structures are transformed through transition states to product complexes that break down to yield alkylated products plus a bromide ion. Calculations using the B3LYP functional indicate that the product complex is stabilized with respect to reactants.

Figure 6 shows the results through pathway 2. The differences in this profile compared to that of pathway 1 are that B3LYP and M06-2X displayed classic double-well potential curves with a slight decrease in energy of the reactant complex (B3LYP, −4.1 kJ mol$^{-1}$; M06-2X, −13.6 kJ mol$^{-1}$). Based on B3LYP and M06-2X results, the reactant complex formed in pathway 1 is less stable than the one formed in pathway 2. The activation energy for reactants proceeding to the transition state is calculated to be lower via pathway 2 using M06-2X but higher using B3LYP.

As shown in Figure 7, the reaction coordinate diagram via the dimeric pathway is similar in shape to that of pathway 2. Both B3LYP and M06-2X indicate a slightly stable reactant complex (B3LYP, −4.2 kJ mol$^{-1}$; M06-2X, −8.6 kJ mol$^{-1}$). The product


DOI: 10.1021/jo502560q
J. Org. Chem. 2015, 80, 2989−3002

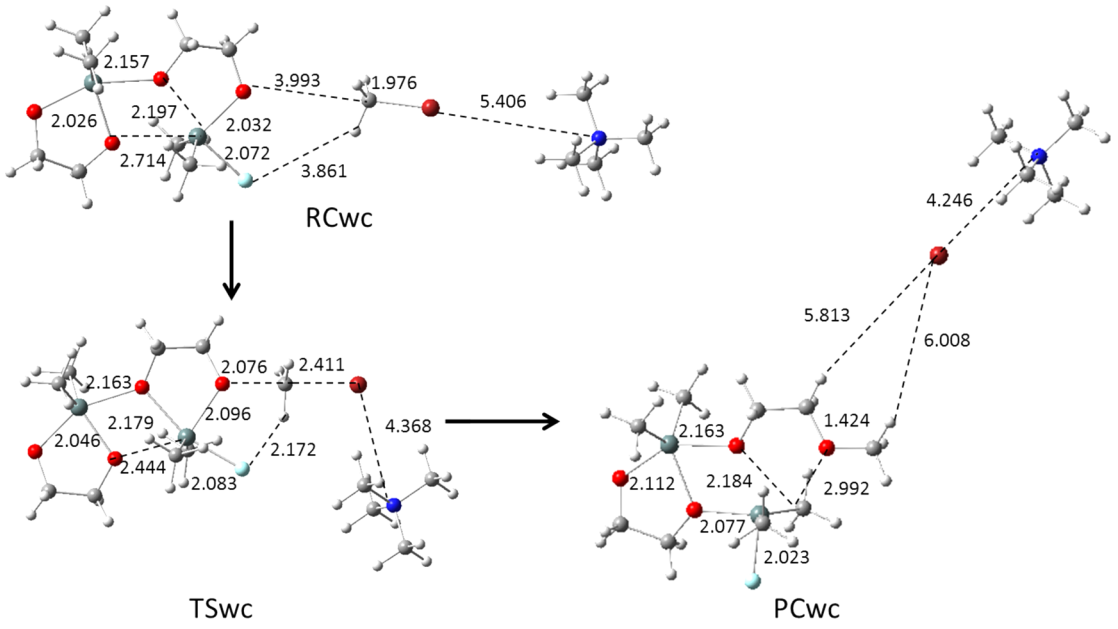


**Figure 12.** Optimized geometries of the alkylation reaction of the monofluoridated dimethylstannylene acetal dimer in the presence of the tetramethylammonium ion in DMF were calculated using the B3LYP/6-311+G(d,p)-LanL2DZdp(Sn) basis set. Reactant complexes, transition states, and product complexes are indicated as RCwc, TSwc, and PCwc. Selected interatomic distances are shown as black numbers (Å).

**Table 10. Selected Interatomic Distances (Å) for Optimized Structures Calculated with M06-2X in DMF**

| | pathway 1 | | | pathway 2 | | | pathway 3 | | |
|---|---|---|---|---|---|---|---|---|---|
| structure | RCcd1 | TScd1 | PCcd1 | RCcd2 | TScd2 | PCcd2 | RCcd | TScd | PCcd |
| $r$(O,H) | 3.484 | | | | | | | | |
| $r$(F,H) | | | | 4.149 | 2.132 | | 3.861 | 2.124 | |
| $r$(O,$C_M$) | 4.460 | 2.058 | 1.427 | 3.992 | 2.016 | 1.422 | 3.993 | 2.032 | 1.417 |
| $r$($C_M$,Br) | 1.982 | 2.315 | 3.598 | 1.976 | 2.362 | 3.746 | 1.976 | 2.353 | 4.387 |
| $r$(Br,N) | 6.315 | 4.169 | 4.113 | 6.094 | 4.214 | 4.111 | 5.406 | 4.162 | 4.113 |
| $r$(H,Br) | | | | | | | | | 3.710 |
| $r$(H′,Br) | | | | | | | | | 3.851 |

complex is only favorable from B3LYP results, while the products were about 40 kJ $mol^{-1}$ higher in energy than that of the reactants. Table 5 summarizes the activation energies and reaction energies for each pathway calculated by various theoretical methods. The dimeric pathway is less favorable than the monomeric pathways due to its higher activation energy.

**Solvent Effects.** Reactions were studied in two different solvents, DMF and water, using B3LYP and M06-2X. The geometries obtained by optimizing the gas-phase structures in media with the bulk dielectric constants of these solvents had structures similar to those calculated in the gas phase (Figure 8 and Table 10). However, several differences were observed. First, the hydrogen bond distance was calculated to be ~0.2 Å longer in the reactant complexes. Second, for the product complexes, the leaving bromide ion retained the position expected in an $S_N2$ reaction, in the line of the C−O bond, where the carbon atom is from methyl bromide. The distance between this carbon atom and the bromide ion in these complexes is usually greater than 5 Å, and no hydrogen bonds were observed. Geometries in water and calculated by M06-2X in DMF were similar to those in DMF (Table 6).

Thermochemical results are shown in Figures 9 and 10. Figure 9 presents the two monomer pathways calculated using the two methods. B3LYP Gibbs energies and all the energetics include ZPVE corrections. In both solvent environments, the reactant complexes were higher in energy than the reactants, 30.2 kJ $mol^{-1}$ (DMF) and 31.0 kJ $mol^{-1}$ (water) for monomer pathway 1 and 17.5 kJ $mol^{-1}$ (DMF) and 21.6 kJ $mol^{-1}$ (water) for monomer pathway 2. RC1 was less stable than RC2, while TS2 was higher in energy than TS1. The product complexes and products in these solvents were more stable relative to reactants than in the gas phase. In comparison of the two monomer pathways, pathway 1 has a lower activation energy. Table 7 summarizes the thermochemical results for the entire process for each pathway.

In solution, the dimer pathway did not have the typical gas-phase double-well shape either, in that the formation of the RC was endothermic by 17.5 kJ $mol^{-1}$ (DMF) and 21.6 kJ $mol^{-1}$ (water). B3LYP provided similar results for both solvent environments. The only obvious difference is the prediction for the relative energy of the PC, which is slightly unstable in water, relative to separated products.

By comparing the reaction barriers and reaction energies (Table 7) of the monomer and dimer pathways, it was found that the monofluoridated monomer and the monofluoridated dimer show similar activities in accelerating the alkylation of diols. If the values calculated are close to reality, the populations of the individual species may influence the


DOI: 10.1021/jo502560q
J. Org. Chem. 2015, 80, 2989−3002

**Table 11. Summary of Activation Energies from Reactant Complexes ($\Delta G^{\ddagger}_1$), Reaction Energies ($\Delta G_{rxn}$), and Overall Activation Energies ($\Delta G^{\ddagger}_0$) for Each Reaction Pathway Calculated in DMF and in Water in the Presence of a Tetramethylammonium Ion**

| pathway | solvent (method) | $\Delta G^{\ddagger a}$ (kJ mol$^{-1}$) | $\Delta G_{rxn}{}^{b}$ (kJ mol$^{-1}$) | $\Delta G^{\ddagger c}$ (kJ mol$^{-1}$) |
|---|---|---|---|---|
| monomer pathway 1 | DMF (B3LYP) | 53.6 | −82.9 | 95.4 |
| | water (B3LYP) | 54.4 | −89.4 | 84.2 |
| | DMF (M06-2X) | 47.3 | −96.8 | 99.4 |
| monomer pathway 2 | DMF (B3LYP) | 72.8 | −41.6 | 99.5 |
| | water (B3LYP) | 77.4 | −66.7 | 92.1 |
| | DMF (M06-2X) | 69.5 | −49.5 | 102.8 |
| dimer pathway | DMF (B3LYP) | 64.8 | −62.0 | 95.3 |
| | water (B3LYP) | 76.6 | −60.9 | 103.6 |
| | DMF (M06-2X) | 70.0 | −73.6 | 102.6 |

[a]Gibbs energy difference between transition states and corresponding reactant complexes. [b]Gibbs energy difference between products and reactants. [c]Gibbs energy difference between transition states and corresponding reactants.

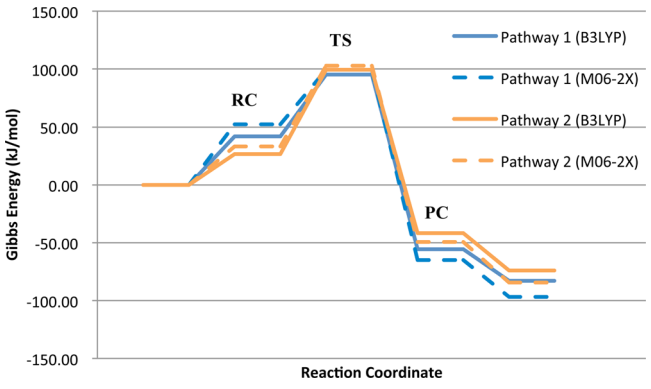


**Figure 13.** Potential energy profile for the pathway of the alkylation reaction via a monomeric intermediate with the tetramethylammonium ion in DMF and calculated using the B3LYP/6-311+G(d,p)-LanL2DZdp(Sn) basis set and M06-2X/6-311+G(d,p)-LanL2DZdp(Sn). For abbreviations, see Figure 5.

pathways followed as suggested earlier, based on gas-phase results.[39]

**Alkylation of Diols in the Presence of a Tetramethylammonium Ion.** The three reaction pathways were modeled with consideration of solvent effects (in DMF and water) and the presence of the tetramethylammonium ion using the B3LYP and M06-2X methods. A difficulty with evaluating the effects of a cation on these reactions is in determining the best location for the ion. The results of calculations of Mulliken charge distribution on a fluoridated monomer (without a cation) calculated in DMF indicated that the fluorine atom and then the two oxygen atoms ($O_e$ and $O_a$) carry the most negative electron density (Table 8). Since fluoride possesses the most negative charge in the system without a cation, the cation was placed adjacent to the fluoride initially. During optimization, the cation stayed close to the fluoride. According

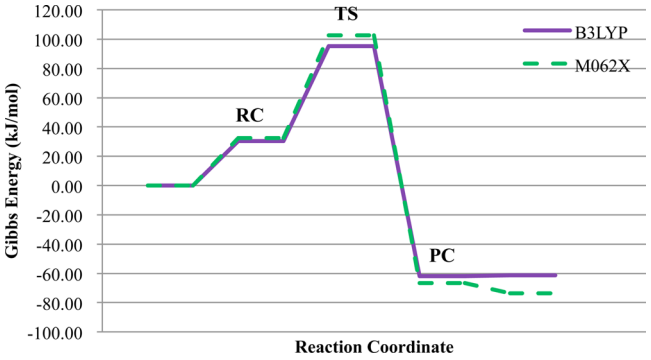


**Figure 14.** Potential energy profile for the pathway of the alkylation reaction via a dimeric intermediate with the tetramethylammonium ion in DMF and calculated using the B3LYP/6-311+G(d,p)-LanL2DZdp-(Sn) basis set and M06-2X/6-311+G(d,p)-LanL2DZdp(Sn). For abbreviations, see Figure 5.

to the molecular modeling simulations, the reaction mechanism is proposed as follows. The electrophile methyl bromide could come from either side and approach one of the nucleophilic oxygens. In the process of the alkylation, negative charge shifts to the bromine atom as the C−Br bond cleaves. The cation moves to the bromine atom as it assumes more electron density. Attraction of the bromine atom by the cation accelerates the bond breakage between the carbon and the increasingly negative bromine atom.

Geometries of monomeric pathways in DMF optimized using B3LYP and their selected geometric data are shown in Figure 11 and Table 9.

Optimized structures including their geometric data through the dimeric pathway using B3LYP are shown in Figure 12.

Based on the changes in interatomic distances on proceeding from reactant complexes to transition states to product complexes in DMF with a tetramethylammonium ion present (see Table 9 and Figure 12), the reacting Sn−O bond is 16, 6, and 7% cleaved in the transition states of pathways 1, 2, and 3, respectively. In contrast, the C−O bond in the transition state is 60, 75, and 75% formed in the transition states of pathways 1, 2, and 3, respectively. These values are similar to the gas-phase results discussed earlier, in which it was observed that the reaction follows pathways which can be described as close to the "electrophile addition first" scenario. One difference with the gas-phase result was noted on the dimer pathway, where the intramolecular Sn−O bond to the fluoride-coordinated tin atom did not lengthen as it had in the gas phase.

The thermodynamic results for the three pathways in DMF with an added tetramethylammonium ion are summarized in Table 11. If the overall activation energies ($\Delta G^{\ddagger}_0$) are compared, it can be seen that monomer pathways in which the apical oxygen in the nucleophile and the dimer pathway are almost equi-energetic (difference of 0.1 kJ mol$^{-1}$ by B3LYP and 3.1 kJ mol$^{-1}$ by M06-2X). Monomer pathway 2, in which the equatorial oxygen is the nucleophile, is somewhat less favorable (Figure 13).

**Evaluation of the "Sn−O Cleavage First" Pathway.** Because a number of authors[6,7,40−42] suggested that the mechanisms of these reactions involve cleavage of a Sn−O bond before formation of the bond to the electrophile, we considered it important to consider this pathway carefully. Because of the creation of a localized charge on an oxygen atom, this route should become more favorable in a polar


DOI: 10.1021/jo502560q
J. Org. Chem. 2015, 80, 2989−3002

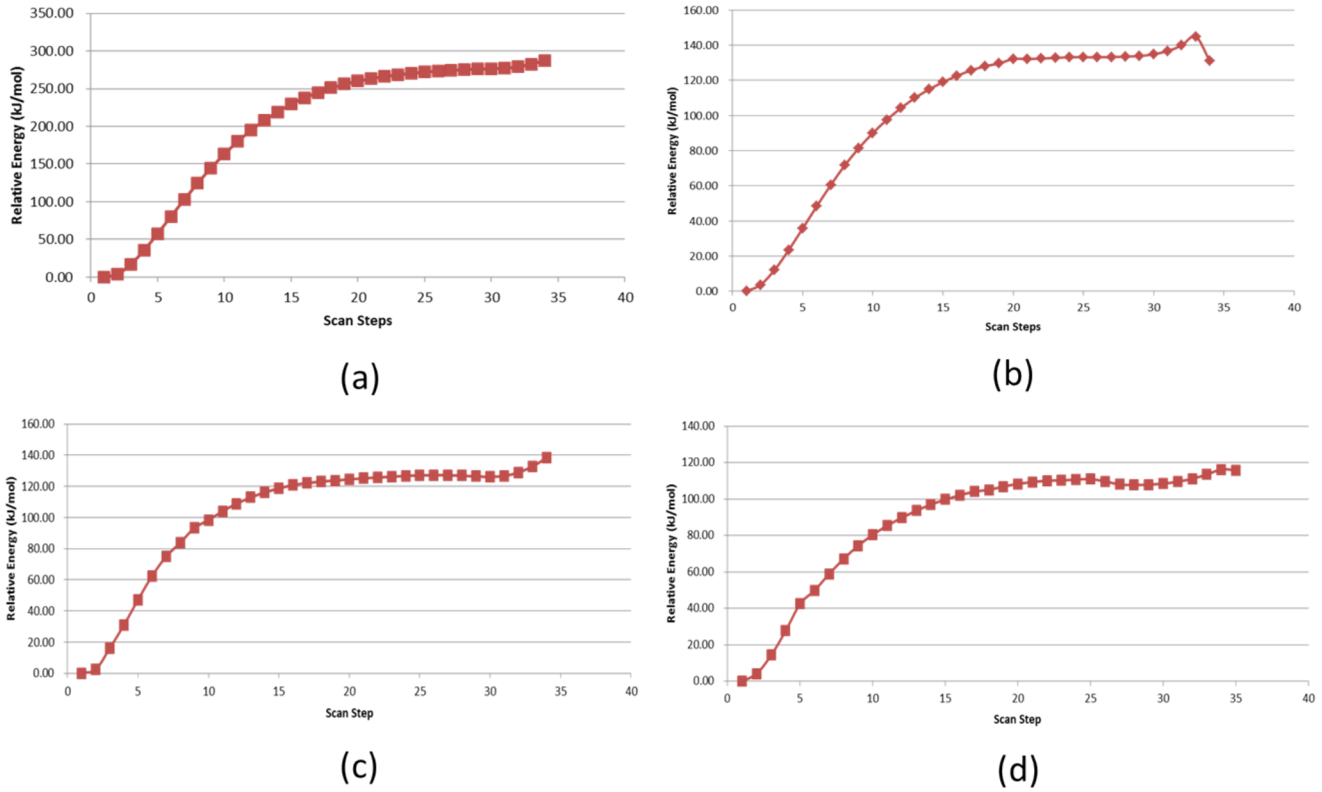


**Figure 15.** Energy scans of Sn−$O_a$ bond cleavages in 0.1 Å steps for the dimethylstannylene acetal for (a) the monomer without a fluoride ion added to tin, (b) the monomer with a fluoride ion added to tin, (c) the monomer with a fluoride ion added to tin and with a tetramethylammonium ion close to the leaving $O_a$ atom, and (d) the dimer with a fluoride ion added to the tin.

environment. Hence, we have evaluated it in DMF and in DMF in the presence of a counterion. The Sn−$O_a$ was stretched in 0.1 Å steps until bond cleavage occurred as measured by the leveling off of the increase in energy. In these energy scan jobs, structures were optimized in each step, and all the structures were evaluated by the restricted B3LYP method to exclude radical pathways. Figure 15 shows the results.

The changes in energy as the Sn−$O_a$ bond is elongated heterolytically were calculated for monomeric dimethylstannylene acetal without a fluoride ion added to tin, with a fluoride ion added to tin, and for the fluoridated monomer in the presence of a tetramethylammonium ion located close to the leaving oxygen anion (Figure 15a−c). In addition, the same calculation was performed for the monofluoridated dimer (Figure 15d). The shapes of the curves obtained resemble those for calculations of bond dissociation energies with a gradual rise in energy as the Sn−$O_a$ bond distance increases until a plateau is reached. If the oxygen anion were the intermediate, it is expected that after an initial increase in energy the system would decrease in energy to a second minimum.

These curves can be used to estimate heterolytic Sn−O bond dissociation energies. The heterolytic Sn−O bond dissociation energy in the monomer is about 280 kJ $mol^{-1}$, while that of the monofluoridated monomer is 138 kJ $mol^{-1}$, which decreases somewhat to about 123 kJ $mol^{-1}$ when a tetramethylammmonium ion is present. The Sn−O bond dissociation energy in the monofluoridated dimer is about 105 kJ $mol^{-1}$. Adding a fluoride ion to tin in the monomer reduces the energy required to break the Sn−O bond heterolytically to about one-half of the original value, and complexation with a tetramethylammonium ion reduces it slightly more. However, there is no indication in any of these calculations that a second minimum is reached in which an anionic oxygen atom is released from the tin atom. Therefore, in the alkylation reaction, bond formation from the reacting oxygen atom to the electrophile is required before Sn−O bond cleavage becomes significant.

## CONCLUSION

The equilibria of the dimethylstannylene acetal of ethylene glycol with fluoride were examined in the gas phase, in DMF solution, and in a DMF solution containing tetramethylammonium ions to extend the gas-phase results of Whittleton at al. for dibutylstannylene acetals.[39] Our results in the gas phase are similar except that we were unable to find a structure for the difluoridated dimer that was a minimum.[39] In DMF, the Gibbs energy for the addition of fluoride to the monomer decreases to about one-third of the gas-phase value but is still substantial. In the presence of a cation in DMF, the equilibrium of the monomer and the fluoridated monomer with the monofluoridated dimer was calculated to lie in favor of the monomeric species. The tetrabutylammonium cation remains close to the most electronegative atom, F, in the optimized structures.

Through IRC and scan calculations, a mechanism of the organotin-mediated alkylation of diols is proposed in the following. In the gas phase, a hydrogen bond leads to the first step of the reaction, but this plays no role in the reaction in DMF with a cation present. In the key step, the nucleophilic oxygen atom participates in a standard $S_N2$ reaction with methyl bromide that is only accompanied by very slight elongation of the Sn−O bond involving the nucleophilic oxygen atom. Thus, this mechanism is close to an "electrophile


DOI: 10.1021/jo502560q
J. Org. Chem. 2015, 80, 2989−3002

addition first" route. The differences calculated between the activation energies for the two fluoridated monomer pathways are small, although the apical oxygen atom of the fluoride-coordinated monomer is calculated to be slightly more reactive than the equatorial oxygen atom of the fluoride-coordinated monomer by both methods. The activation energy for the dimer pathway is similar to that for the apical oxygen monomer pathway.

An evaluation of "Sn−O bond cleavage first" pathway was performed by using scan jobs to test the effect of progressive heterolytic Sn−O bond dissociation on energy for the various species in DMF. The energy increased as the bond was elongated until a plateau was reached, identical to what would be expected for a heterolytic bond dissociation. No second minima were found corresponding to a dissociated oxygen anion. The addition of fluoride to tin was found to cut the heterolytic Sn−O bond dissociation energy in half, but the calculated heterolytic bond dissociation energy was still >100 kJ $mol^{-1}$, indicating that the reaction does not follow a "Sn−O bond cleavage first" pathway.

Jenkins and Potter observed that alkylation of the dibutylstannylene acetal of methyl 4,6-*O*-benzylidene-α-D-glucopyranoside favored 3-O-substitution when the dibutylstannylene acetal was activated by fluoride but 2-O-substitution when activated by iodide or just by heating.[65] The above results suggest that this change in product distribution was caused by a change in the intermediates involved from fluoridated monomer to dimer or iodinated dimer. Calculations are underway to evaluate this suggestion.

## ■ ASSOCIATED CONTENT

### Supporting Information

Archive entries for all geometry optimizations. This material is available free of charge via the Internet at http://pubs.acs.org.

## ■ AUTHOR INFORMATION


### Corresponding Authors

*E-mail russell.boyd@dal.ca. Telephone: 902-494-8883. Fax: 902-494-1310.

*E-mail: bruce.grindley@dal.ca. Telephone: 902-494-2041. Fax: 902-494-1310.


### Notes

The authors declare no competing financial interest.

## ■ ACKNOWLEDGMENTS

We thank the Natural Sciences and Engineering Research Council of Canada (NSERC) for financial support. We gratefully acknowledge ACEnet, the regional high performance computing consortium for universities in Atlantic Canada. ACEnet is funded by the Canada Foundation for Innovation (CFI), the Atlantic Canada Opportunities Agency (ACOA), and the Provinces of Newfoundland & Labrador, Nova Scotia, and New Brunswick.

## ■ REFERENCES


(1) David, S.; Hanessian, S. *Tetrahedron* **1985**, *41*, 643−663.
(2) Grindley, T. B. *Adv. Carbohydr. Chem. Biochem.* **1998**, *53*, 17−142.
(3) Grindley, T. B. In *Tin, Fundamentals and Applications*; Gielen, M., Davies, A. G., Tiekink, E. R. T., Pannell, K. H., Eds.; John Wiley: Chichester, UK, 2008; pp 491−508.
(4) David, S. *C. R. Acad. Sci., Ser. C* **1974**, *278*, 1051−1053.
(5) Wagner, D.; Verheyden, J. P. H.; Moffatt, J. G. *J. Org. Chem.* **1974**, *39*, 24−30.
(6) Dong, H.; Zhou, Y.; Pan, X.; Cui, F.; Liu, W.; Liu, J.; Ramström, O. *J. Org. Chem.* **2012**, *77*, 1457−1467.
(7) Zhou, Y.; Li, J.; Zhan, Y.; Pei, Z.; Dong, H. *Tetrahedron* **2013**, *69*, 2693−2700.
(8) Bieg, T.; Kral, K.; Paszkowska, J.; Szeja, W.; Wandzik, I. *J. Carbohydr. Chem.* **2012**, *31*, 593−601.
(9) Liang, X.-Y.; Liu, Q.-W.; Bin, H.-C.; Yang, J.-S. *Org. Biomol. Chem.* **2013**, *11*, 3903−3917.
(10) Lou, X. *Asian J. Chem.* **2013**, *25*, 2281−2283.
(11) Lou, X.; Zhao, J. *J. Chin. Chem. Soc.* **2012**, *59*, 1111−1118.
(12) Picard, S.; Crich, D. *Tetrahedron* **2013**, *69*, 5501−5510.
(13) Xia, L.; Lowary, T. L. *J. Org. Chem.* **2013**, *78*, 2863−2880.
(14) Dvorakova, M.; Nencka, R.; Dejmek, M.; Zbornikova, E.; Brezinova, A.; Pribylova, M.; Pohl, R.; Migaud, M. E.; Vanek, T. *Org. Biomol. Chem.* **2013**, *11*, 5702−5713.
(15) Muramatsu, W.; Takemoto, Y. *J. Org. Chem.* **2013**, *78*, 2336−2345.
(16) Muramatsu, W. *J. Org. Chem.* **2012**, *77*, 8083−8091.
(17) Demizu, Y.; Kubo, Y.; Miyoshi, H.; Maki, T.; Matsumura, Y.; Moriyama, N.; Onomura, O. *Org. Lett.* **2008**, *10*, 5075−5077.
(18) Martinelli, M. J.; Vaidyanathan, R.; Pawlak, J. M.; Nayyar, N. K.; Dhokte, U. P.; Doecke, C. W.; Zollars, L. M. H.; Moher, E. D.; van Khau, V.; Kosmrlj, B. *J. Am. Chem. Soc.* **2002**, *124*, 3578−3585.
(19) Lee, D.; Taylor, M. S. *Synthesis* **2012**, *44*, 3421−3431.
(20) Voight, E. A.; Rein, C.; Burke, S. D. *J. Org. Chem.* **2002**, *67*, 8489−8499.
(21) Giordano, M.; Iadonisi, A. *J. Org. Chem.* **2014**, *79*, 213−222.
(22) Xu, H.; Lu, Y.; Zhou, Y.; Ren, B.; Pei, Y.; Dong, H.; Pei, Z. *Adv. Synth. Catal.* **2014**, *356*, 1735−1740.
(23) Smith, P. J.; White, R. F. M.; Smith, L. *J. Organomet. Chem.* **1972**, *40*, 341−353.
(24) Whittleton, S. R.; Rolle, A. J.; Boyd, R. J.; Grindley, T. B. *Organometallics* **2010**, *29*, 6384−6392.
(25) David, S.; Pascard, C.; Cesario, M. *Nouv. J. Chim.* **1979**, *3*, 63−68.
(26) Davies, A. G.; Price, A. J.; Dawes, H. M.; Hursthouse, M. B. *J. Chem. Soc., Dalton Trans.* **1986**, 297−302.
(27) Plasseraud, L.; Ballivet-Tkatchenko, D.; Cattey, H.; Chambrey, S.; Ligabue, R.; Richard, P.; Willem, R.; Biesemans, M. *J. Organomet. Chem.* **2010**, *695*, 1618−1626.
(28) Grindley, T. B.; Thangarasa, R.; Bakshi, P. K.; Cameron, T. S. *Can. J. Chem.* **1992**, *70*, 197−204.
(29) Grindley, T. B.; Wasylishen, R. E.; Thangarasa, R.; Power, W. P.; Curtis, R. D. *Can. J. Chem.* **1992**, *70*, 205−217.
(30) Bates, P. A.; Hursthouse, M. B.; Davies, A. G.; Slater, S. D. *J. Organomet. Chem.* **1989**, *363*, 45−60.
(31) Cameron, T. S.; Bakshi, P. K.; Thangarasa, R.; Grindley, T. B. *Can. J. Chem.* **1992**, *70*, 1623−1630.
(32) Holzapfel, C. W.; Koekemoer, J. M.; Marais, C. F.; Kruger, G. J.; Pretorius, J. A. *S. Afr. J. Chem.* **1982**, *35*, 80−88.
(33) Grindley, T. B.; Thangarasa, R. *J. Am. Chem. Soc.* **1990**, *112*, 1364−1373.
(34) Grindley, T. B.; Thangarasa, R. *Can. J. Chem.* **1990**, *68*, 1007−1019.
(35) Kong, X.; Grindley, T. B. *Can. J. Chem.* **1994**, *72*, 2405−2415.
(36) David, S.; Thiéffry, A.; Veyrières, A. *J. Chem. Soc., Perkin Trans. 1* **1981**, 1796−1801.
(37) Danishefsky, S. J.; Hungate, R. *J. Am. Chem. Soc.* **1986**, *108*, 2486−2487.
(38) Nagashima, N.; Ohno, M. *Chem. Lett.* **1987**, 141−144.
(39) Whittleton, S. R.; Boyd, R. J.; Grindley, T. B. *J. Phys. Chem. A* **2013**, *117*, 12648−12657.
(40) Alais, J.; Veyrières, A. *J. Chem. Soc., Perkin Trans. 1* **1981**, 377−381.
(41) Nagashima, N.; Ohno, M. *Chem. Pharm. Bull.* **1991**, *39*, 1972−1982.




DOI: 10.1021/jo502560q
*J. Org. Chem.* 2015, 80, 2989−3002

(42) Harpp, D. N.; Gingras, M. *J. Am. Chem. Soc.* **1988**, *110*, 7737−7745.
(43) Wakamatsu, K.; Orita, A.; Otera, J. *Organometallics* **2008**, *27*, 1092−1097.
(44) Kalhor, M. P.; Chermette, H.; Ballivet-Tkatchenko, D. *Polyhedron* **2012**, *32*, 73−77.
(45) Wakamatsu, K.; Orita, A.; Otera, J. *Organometallics* **2010**, *29*, 1290−1295.
(46) Kalhor, M. P.; Chermette, H.; Chambrey, S.; Ballivet-Tkatchenko, D. *Phys. Chem. Chem. Phys.* **2011**, *13*, 2401−2408.
(47) Frisch, M. J.; Trucks, G. W.; Schlegel, H. B.; Scuseria, G. E.; Robb, M. A.; Cheeseman, J. R.; Scalmani, G.; Barone, V.; Mennucci, B.; Petersson, G. A.; Nakatsuji, H.; Caricato, M.; Li, X.; Hratchian, H. P.; Izmaylov, A. F.; Bloino, J.; Zheng, G.; Sonnenberg, J. L.; Hada, M.; Ehara, M.; Toyota, K.; Fukuda, R.; Hasegawa, J.; Ishida, M.; Nakajima, T.; Honda, Y.; Kitao, O.; Nakai, H.; Vreven, T.; Montgomery, J. A., Jr.; Peralta, J. E.; Ogliaro, F.; Bearpark, M.; Heyd, J. J.; Brothers, E.; Kudin, K. N.; Staroverov, V. N.; Kobayashi, R.; Normand, J.; Raghavachari, K.; Rendell, A.; Burant, J. C.; Iyengar, S. S.; Tomasi, J.; Cossi, M.; Rega, N.; Millam, J. M.; Klene, M.; Knox, J. E.; Cross, J. B.; Bakken, V.; Adamo, C.; Jaramillo, J.; Gomperts, R.; Stratmann, R. E.; Yazyev, O.; Austin, A. J.; Cammi, R.; Pomelli, C.; Ochterski, J. W.; Martin, R. L.; Morokuma, K.; Zakrzewski, V. G.; Voth, G. A.; Salvador, P.; Dannenberg, J. J.; Dapprich, S.; Daniels, A. D.; Farkas, O.; Foresman, J. B.; Ortiz, J. V.; Cioslowski, J.; Fox, D. J.*Gaussian 09*, revision C.01; Gaussian, Inc: Wallingford, CT, 2009.
(48) Becke, A. D. *J. Chem. Phys.* **1993**, *98*, 5648−5652.
(49) Becke, A. D. *J. Chem. Phys.* **1993**, *98*, 1372−1377.
(50) Lee, C. H.; Yang, W.; Parr, R. G. *Phys. Rev. B* **1988**, *37*, 785−789.
(51) Check, C. E.; Faust, T. O.; Bailey, J. M.; Wright, B. J.; Gilbert, T. M.; Sunderlin, L. S. *J. Phys. Chem. A* **2001**, *105*, 8111−8116.
(52) Wadt, W. R.; Hay, P. J. *J. Chem. Phys.* **1985**, *82*, 284−298.
(53) Peng, C. Y.; Schlegel, H. B. *Isr. J. Chem.* **1993**, *33*, 449−454.
(54) Peng, C. Y.; Ayala, P. Y.; Schlegel, H. B.; Frisch, M. J. *J. Comput. Chem.* **1996**, *17*, 49−56.
(55) Gonzalez, C.; Schlegel, H. B. *J. Chem. Phys.* **1989**, *90*, 2154−2161.
(56) Gonzalez, C.; Schlegel, H. B. *J. Phys. Chem.* **1990**, *94*, 5523−5527.
(57) Frisch, M. J.; Head-Gordon, M.; Pople, J. A. *Chem. Phys. Lett.* **1990**, *166*, 275−280.
(58) Head-Gordon, M.; Pople, J. A.; Frisch, M. J. *Chem. Phys. Lett.* **1988**, *153*, 503−506.
(59) Frisch, M. J.; Head-Gordon, M.; Pople, J. A. *Chem. Phys. Lett.* **1990**, *166*, 281−289.
(60) Head-Gordon, M.; Head-Gordon, T. *Chem. Phys. Lett.* **1994**, *220*, 122−128.
(61) Zhao, Y.; Truhlar, D. G. *Acc. Chem. Res.* **2008**, *41*, 157−167.
(62) Shi, Z.; Boyd, R. J. *J. Am. Chem. Soc.* **1989**, *111*, 1575−1579.
(63) Shi, Z.; Boyd, R. J. *J. Am. Chem. Soc.* **1990**, *112*, 6789−6796.
(64) Grimme, S. *Angew. Chem., Int. Ed.* **2006**, *45*, 4460−4464.
(65) Jenkins, D. J.; Potter, B. V. L. *Carbohydr. Res.* **1994**, *265*, 145−149.


DOI: 10.1021/jo502560q
*J. Org. Chem.* 2015, 80, 2989−3002